ACS APPLIED MATERIALS & INTERFACES

Research Article

www.acsami.org

Stoichiometry, Length, and Wall Thickness Optimization of TiO_2 Nanotube Array for Efficient Alcohol Sensing

A. Hazra,[†] B. Bhowmik,[†] K. Dutta,[†] P.P. Chattopadhyay,[‡] and P. Bhattacharyya*,[†]

[†]Nano-Thin Films and Solid State Gas sensor Devices Laboratory, Department of Electronics and Telecommunication Engineering and [‡]Department of Metallurgy and Materials Engineering, Indian Institute of Engineering Science and Technology (IIEST), Shibpur, Howrah-711103, India

ABSTRACT: The present study concerns development of an efficient alcohol sensor by controlling the stoichiometry, length, and wall thickness of electrochemically grown TiO_2 nanotube array for its use as the sensing layer. Judicious variation of H_2O content (0, 2, 10 and 100% by volume) in the mixed electrolyte comprising ethylene glycol and NH_4F resulted into the desired variation of stoichiometry. The sensor study was performed within the temperature range of 27 to 250 °C for detecting the alcohols in the concentration range of 10−1000 ppm. The nanotubes grown with the electrolyte containing 2 vol % H_2O offered the maximum response magnitude. For this stoichiometry, variation of corresponding length (1.25−2.4 μm) and wall thickness (19.8−9 nm) of the nanotubes was achieved by varying the anodization time (4−16 h) and temperatures (42−87 °C), respectively. While the variation of length influenced the sensing parameters insignificantly, the best response magnitude was achieved for ~13 nm wall thickness. The underlying sensing mechanism was correlated with the experimental findings on the basis of structural parameters of the nanotubes.

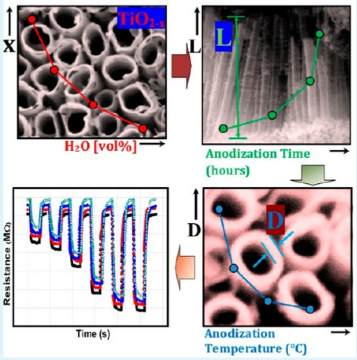

KEYWORDS: *TiO_2 nanotubes, stoichiometry, length, wall thickness, optimization, alcohol sensing*

INTRODUCTION

Electrochemically grown ordered and self-organized TiO_2 nanotubular structures with high aspect ratio have been found to be the potential high bandgap semiconductor for sensor applications owing to their unique physical, chemical, and electronic properties.[1−4]

TiO_2 nanotube-based sensors have extensively been stuided for the detection of oxygen and hydrogen.[4−9] However, very few reports are available on TiO_2 nanotube-based alcohol sensors.[5−7] Kwon et al. have reported the TiO_2 nanotube-based ethanol sensor at 250 °C that yielded the response time and recovery time of 90 and 14 s, respectively.[5] Perillo et al. have developed TiO_2 nanotubes with variable diameter and thickness for ethanol sensing at room temperature. The aforesaid attempt exhibited sensors with relatively poor sensitivity and sluggish response (~13 min) and recovery (~3 min).[6] Kılınç et al. studied ethanol and methanol sensing with TiO_2 nanotubes with varying nanotube morphology achieved by variation of applied potential, temperature, and the type of electrolytes. However, such sensors exhibited relatively poor response magnitude for ethanol (16%) and methanol (10%) at 5000 ppm. The response and recovery times were also found to be extremely high (as high as 12 and 30 min, respectively, toward 5000 ppm ethanol at 200 °C).[7]

Scrutiny of the literature reveals that the earlier attempts of enhancing the sensing parameters by controlling the nanotube structure have not considered some of the pivotal parameters like (i) concentrations of oxygen vacancy (V_o) of the nanotubes, (ii) tube radius, (iii) tube wall thickness, (iv) wall separation, and (v) tube length in a systemayic manner to improve the sensor performance.[5−7] As the TiO_2 nanotube growth (anodic) is a concomitant process of (i) oxide formation and (ii) oxide dissolution, naotube structure is strongly dependent on the competitive kinetics of the reactions.[1,10] Recently, the authors have reported the effect of stoichiometry of TiO_2 nanotube array on the room-temperature alcohol sensing.[11] However, the response of such a device at higher temperatures (and at optimum temperature) was not discussed. Moreover, the variation of other structural attributes like length and wall thickness of the nanotubes on alcohol sensing was not addressed.

To bridge the gap, three key attributes of nanotube array, namely, stoichimetry (oxygen vacancy), length, and wall thickness of the nanotube were systematically controlled in the present report to achieve efficient alcohol sensing. Stoichiometry of the nanotube was first varied by varying the H_2O content (0, 2, 10, and 100% by volume) in the mixed electrolyte consisting of NH_4F and ethelyne glycol. The maximum response for alcohol sensing was achieved for the nanotubes grown with 2 vol % H_2O. Subsequently, the lengths of the nanotubes were varied maintaining the fixed stoichiometry. Finally, the nanotube wall thicknesses were varied by vayring the anodization temperatures. Among the different structures grown under the selective variation of process schedule, nanotube array with 13 nm wall thickness offered the most promising sensor characteristics.

Received: July 30, 2014
Accepted: April 16, 2015
Published: April 28, 2015

DOI: 10.1021/acsami.5b01785

Table 1. Details of the Anodization Parameters for Three Different Sets of TiO_2 Nanotubes

	set (1) variation of oxygen vacancies (V_O)		set (2) variation of tube lengths (L)		set (3) variation of wall thicknesses (D)	
	anodization time: 2 h temperature: 27 °C		temperature: 27 °C electrolyte: EG + 2 vol % H_2O		electrolyte: EG + 2 vol % H_2O anodization time: 2 h	
serial no.	sample no.	electrolyte composition	sample no.	anodization time	sample no.	temperature
1	TN_1	EG + 0 vol % H_2O	L_1	4 h	D_1	42 °C
2	TN_2	EG + 2 vol % H_2O	L_2	8 h	D_2	57 °C
3	TN_3	EG + 10 vol % H_2O	L_3	12 h	D_3	72 °C
4	TN_4	100 vol % H_2O	L_4	16 h	D_4	87 °C

■ EXPERIMENTAL SECTION

High-purity titanium foil (0.25 mm, 99.5%) was thoroughly cleaned and subsequently rinsed for use as the substrate. Electrochemical anodization was performed using two electrode configurations (electrode separation ~4 cm). Cylindrical-shaped graphite electrode (radius: 0.25 cm, surface area: 8.547 cm^2) was used as the cathode, and Ti foil was used as the anode. Room-temperature anodization process was performed with 20 V constant potential. The current through the electrolyte was continuously recorded during the anodization process.[1,10]

Electrolyte composition for developing the TiO_2 nanotube array with variable oxygen vacancy content was discussed in our earlier report.[11] H_2O contents were chosen to be 0, 2, 5, and 100 vol % in the mixed electrolyte consisting of 0.5 wt % NH_4F and ethylene glycol. Anodization was performed for 2 h at room temperature (27 °C). Values of the structural parameters for 5 vol % H_2O follows the similar trends (as revealed from Figure 2a) as that of 0−100 vol % cases. No significant improvement in sensing performance was observed for the TiO_2 nanotube sensor with 5 vol % H_2O. Therefore, the other structural results and sensor results for 5 vol % case were omitted.

TiO_2 nanotubes with variable tube lengths (L) were synthesized by varying the anodization time (4, 8, 12, and 16 h) using the electrolyte composition of 0.5 wt % NH_4F + ethylene glycol + 2 vol % H_2O at 27 °C. Similar electrolyte composition was used for the synthesis of TiO_2 nanotubes (with variable tube wall thicknesses (D)) by varying the anodization temperatures (42, 57, 72, and 87 °C), for a constant anodization time of 2 h. The details of the anodization parameters for three different sets of TiO_2 nanotubes are summarized in Table 1.

Three sets of TiO_2 nanotubes, treated under different schedules (i.e., TN_1−TN_4, D_1−D_4, and L_1−L_4) were annealed at 300 °C for 4 h in a closed annealing furnace maintaining the oxygen partial pressure at ~4 kPa.

Morphology and crystal structures of the annealed TiO_2 nanotubes were characterized by using field emission scanning electron microscopy (FESEM) and X-ray diffraction (XRD, $\lambda = 1.54$ Å) analyses, respectively. Presence of oxygen vacancies (V_o) in the TiO_2 nanotube samples (TN_1 to TN_4) was studied by photoluminescence (PL) spectroscopy. Electrical characterizations of the TiO_2 nanotube sensor layer were performed by using electrochemical capacitance voltage (ECV) measurement at 0.138 kHz alternating current frequency in 0.1 M NaOH aqueous electrolyte solution.

Palladium contact electrodes (2 mm × 2 mm × 40 nm) were deposited on the 7 mm × 3 mm TiO_2 nanotube array (electrode separation: 2 mm) by e-beam evaporation (~1 × 10^6 mbar) technique.[2,11]

The vapor sensor measurement technique has earlier been reported by the authors.[2] The sensor response magnitude (RM) is defined as the ratio of change in sensor resistance in the presence of alcohol vapor $[(R_a - R_g) = \Delta R]$, and the baseline sensor resistance in air ($R_a = R$) is expressed as RM = $(\Delta R/R)$.[2] The response time of the sensor was calculated as the time taken by the sensor signal to reach 90% of its saturation value upon exposure to alcohol vapor.[5]

■ RESULTS AND DISCUSSION

Variation of Stoichiometry and Structural Parameters.

Stoichiometry. Electrochemically, TiO_2 nanotube formation may be understood as the concomitant process of oxide formation and dissolution.[1] The oxide growth depends on the reaction between Ti metal and H_2O (acidic medium) under the influence of an applied potential. On the other hand, oxide dissolution depends on the soluble titanium fluoride $[TiF_6^{2-}]$ formation (in case of fluorine-based electrolytes) generated through the reaction between the grown oxide and fluoride ions.[12] In the first set of study, H_2O content in the electrolyte was varied during anodization to developed defect (V_o)/stoichiometry controlled TiO_2 nanotubes. Because of the restricted supply of H_2O (or the restricted supply of oxygen) in electrolyte, reduced TiO_2 nanotubes are formed offering a substoichiometric composition[13] that can be represented by the generalized suboxide phase of Ti_nO_{2n-1} ($n = 1, 2, 3\cdots$).

Paucity of H_2O content in the electrolyte (during anodization) eventually restricts the supply of oxygen, which leads to

(i) Reduced TiO_2 formation having different suboxide states (TiO_x) that ensure existence of higher concentrations of V_o (eq 1).[3]

$$Ti^{4+} + xO^{2-} \rightarrow TiO_x(\mathrm{sub} - \mathrm{oxide}) + 2xe^- \qquad (1)$$

(ii) poor nanotubular structure formation due to restricted formation of $[TiF_6^{2-}]$.

Occasionally, fluorine ions directly react with Ti^{4+} and form undissolved $[TiF_6^{2-}]$ due to presence of limited amount of H_2O in the electrolyte. As a result, the ordered TiO_2 nanotube formation is constrained, and the resultant structure evolves as the wall connected nanotube array occasionally covered with nanofiber-like compositions.[14]

Although variation in stoichiometry (or V_O) in TiO_2 nanotube achieved by varying the H_2O contents in the electrolyte during anodization, the technique has the unavoidable influence on the other structural parameters (like tube length) of the TiO_2 nanotubes (Figure 1A). With lowering of the H_2O content, the barrier layer thickness becomes thinner. This results in better ionic conduction (compared to the aqueous electrolyte) and fast movement of metal/oxide (Ti/TiO_2) interface toward metal substrate (Ti), enhancing the TiO_2 nanotube lengths.[14,15]

Length. In the second set of experiments, an attempt was made to synthesize TiO_2 nanotube array with variable tube lengths (L_1 to L_4), maintaining the other tube parameters unaltered, to establish the effect of length variations on the alcohol-sensing performance. Though the lengths of the TiO_2 nanotubes principally depend on four major parameters, namely, (i) H_2O contents in the electrolyte, (ii) concentrations of F^- ion in the electrolyte, (iii) anodization time, and (iv) applied potential,[16,17] only the anodization time was increased from 4 to 16 h to enhance the period of ionic conduction for increasing lengths of the nanotubes. During the process, unintentional

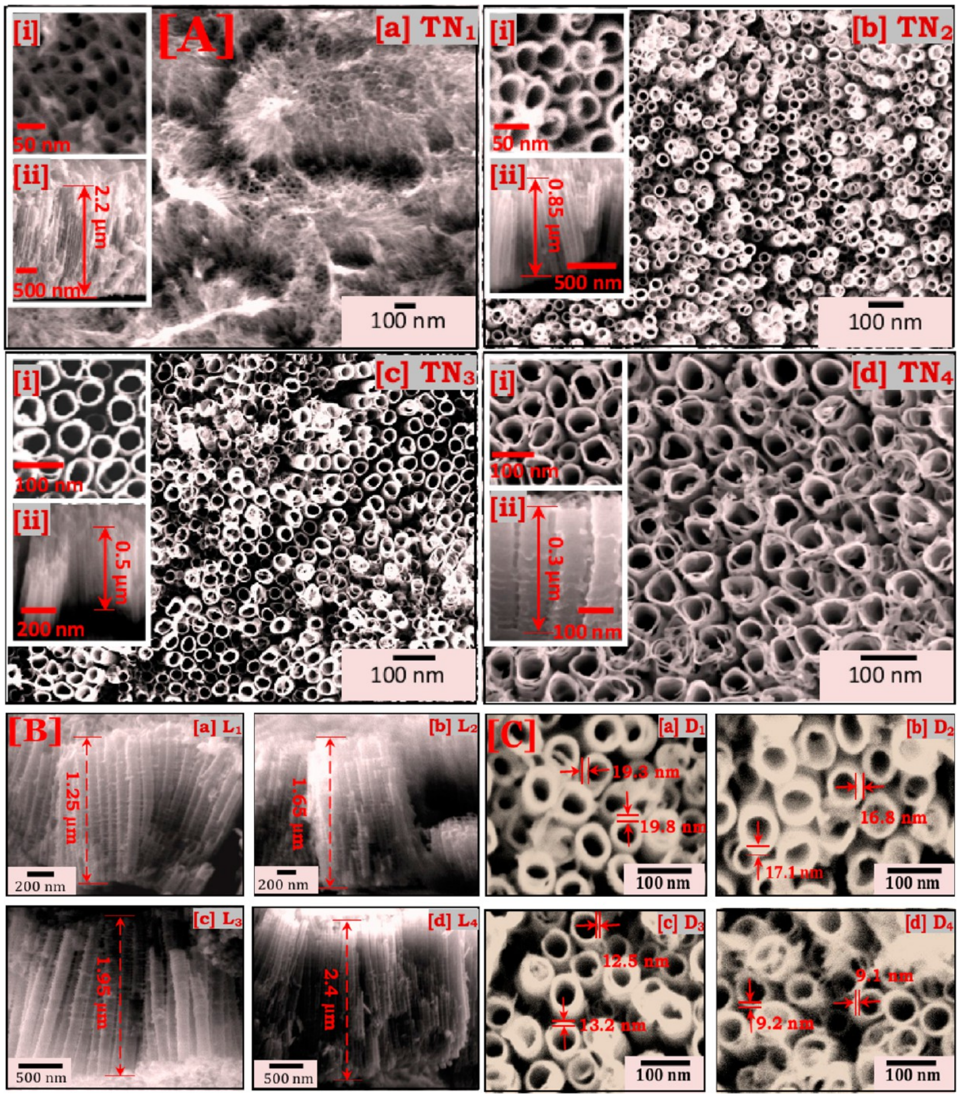

Figure 1. FESEM images of anodically grown four different TiO_2 nanoforms. (A) TiO_2 nanotubes with variable oxygen vacancies (TN_1 to TN_4). (B) Four different TiO_2 nanotubes (L_1 to L_4) with variable tube lengths (L). (C) Four different TiO_2 nanotubes with variable wall thicknesses (D).

variations of the other structural parameters of the TiO_2 nanotubes were found to be insignificant.

Wall Thickness. In the third set of the study, TiO_2 nanotube array was synthesized with variable tube wall thicknesses (D_1 to D_4) keeping all other tube parameters fixed to realize the effect of nanotube wall thickness on the alcohol-sensing performance. Variation of the TiO_2 nanotube wall thickness principally depends on the higher dissolution rate (in horizontal direction) of TiO_2 layer by F^- ions in the electrolyte, which depends on two key factors: (i) higher drift velocity of the F^- ions in the electrolyte[18] and (ii) higher rate of diffusion of F^- ions through the nanotube wall.[19]

According to the Stokes−Einstein relationship $D = kT/6\pi\eta\sigma$, (where D is the diffusion coefficient, k is the Boltzmann's constant, T is the ambient temperature, η is the viscosity of the electrolyte, and σ is the diameter of the spherelike particle), rate of diffusion of F^- ions increases with increase in the anodization temperature (T) leading to the higher rate of dissolution. At higher temperatures, viscosity (η) of the elctrolyte becomes lower and, hence, enhances the velocity of the F^- in the electrolyte. As a result, the rate of oxide dissolution by F^- ions increases, and the nanotube wall thickness (D) is reduced.

Structural Characterizations of the TiO_2 Nanotubes.

Field Emission Scanning Electron Microscopy. The FESEM images as shown in Figure 1A reveal the surface morphology of the grown anodic layers of four TiO_2 samples with variable oxygen vacancies (TN_1 to TN_4). In the absence of H_2O (TN_1), fiberlike nonuniform TiO_2 surface was formed with indistinct (wall-connected) nanotube formation. Surface of TN_1 is partially covered with an initial oxide layer, grown during the first stage of synthesis.[14] Such oxide coverage strongly affects the subsequent nanotube formation. The initial oxide layer was removed significantly in case of TN_2 (2 vol % H_2O) indicating the formation of both wall-connected and wall-separated TiO_2 nanotubes (Figure 1Ab). On the contrary, wall-separated and ordered TiO_2 nanotube array formation is evident in case of TN_3 and TN_4 where no perceptable coverage of oxide layer is observed. Free-standing nature of the nanotubes was found to be more prominent in case of TN_4 compared to that in TN_3. It is evident from the inset of Figure 1A that the tube length (L) decreases monotonically from TN_1 to TN_4 (from 2.2 to 0.3 μm).

TiO_2 nanotubes with variable tube lengths were synthesized by varying the anodization time (from 4 to 16 h). As a result, the nanotube length variations from 1.25 to 2.4 μm were achieved for

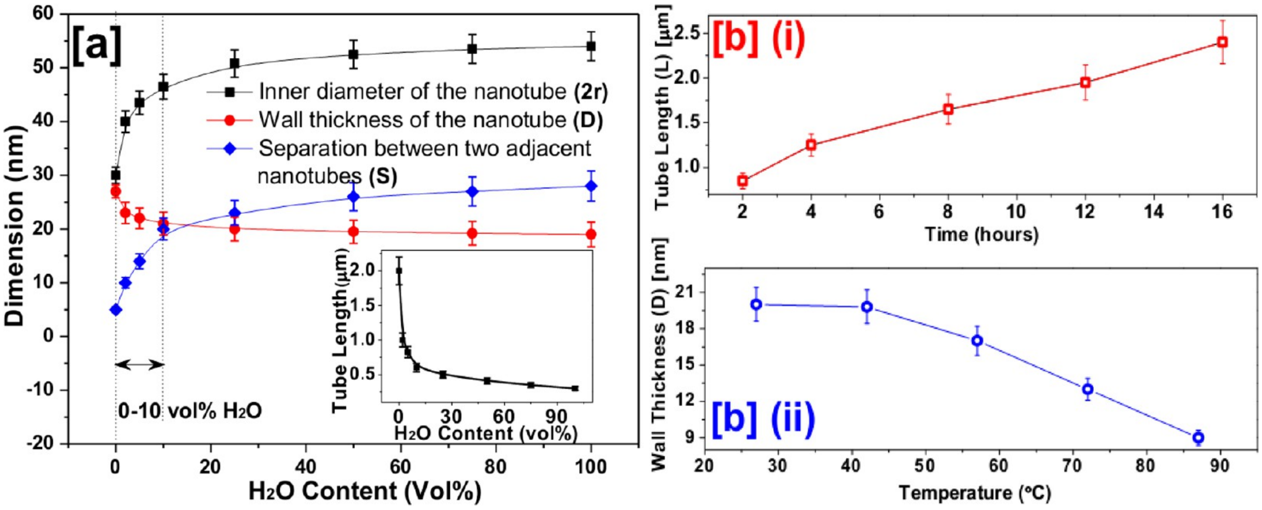

Figure 2. (a) Variations of the structural parameters (inner diameters ($2r$), wall thicknesses (D), and wall separations (S)) of anodically grown TiO_2 nanotubes as a function of H_2O content in the electrolyte (in inset, tube length (L) variations as a function of H_2O content in the electrolyte). (b) (i) Tube length variations (L) as a function of anodization time. (b) (ii) Tube wall thickness (D) variations as a function of anodization temperatures.

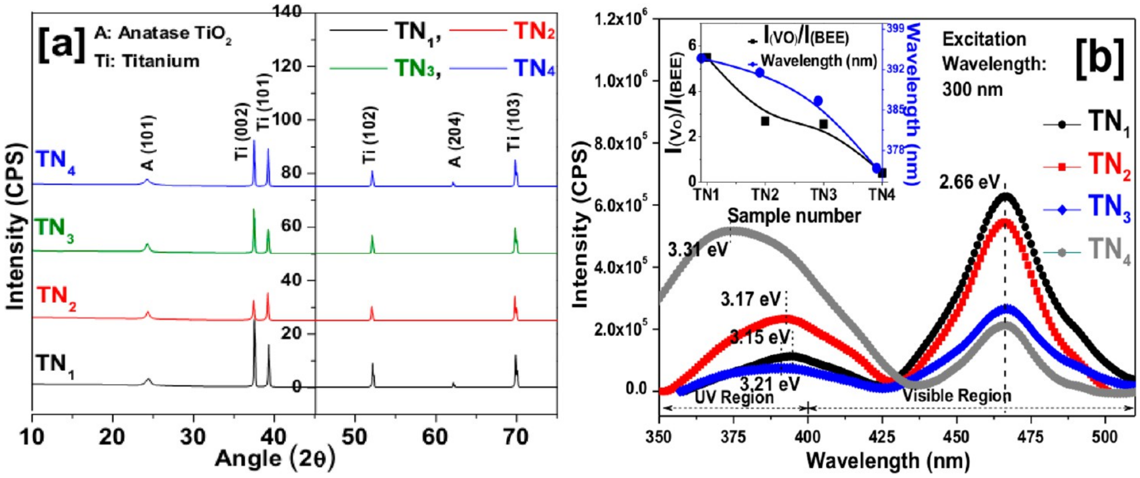

Figure 3. Variation of (a) XRD patterns and (b) PL spectra of four different TiO_2 nanoforms (TN_1 to TN_4) with variable oxygen vacancies (Figure 3b partially reproduced from ref 11 with necessary permission from appropriate authority).

four different samples (L_1 to L_4). Except the anodization time, all the other anodization parameters were identical to that for synthesizing TN_2. Variations of nanotube lengths are clearly evident from FESEM images shown in Figure 1B. The corresponding FESEM images in Figure 1C represent the reduction of the D value from 19.8 to 9 nm (D_1 to D_4) for corresponding increase in anodization temperatures from 42 to 87 °C.

Figure 2a shows the variation of nanotube parameters (e.g., $2r$, D, and S) as a function of H_2O content in the electrolyte during anodization (i.e., TN_1 to TN_4 samples). The maximum variation of the structural parameters (Figure 2a) was observed in the range of 0−10 vol % H_2O with almost imperceptible change in the range of 10−100 vol % H_2O. Within this range, four different H_2O concentrations, namely, 0, 2, 5, and 10 vol %, were considered. Almost no change was observed in the structural parameters between 2 and 5 vol % cases. Figures 2b(i) and 3b(ii) represent the monnotonic incremental and decremental nature of tube lengths (L) and tube wall thicknesses (D) with the variations of anodization time (2−16 h) and anodization temperatures (27 to 87 °C), respectively.

X-ray Diffraction and Photoluminescence Spectroscopy. The chemistry and crystal structure of the TiO_2 samples were identified by XRD analysis as shown in Figure 3a. Anatase (101) crystallinity was common for all the four cases. Some low-intenity anatase (204) peaks were evident only in the case of TN_1 and TN_4. All the patterns (TN_1 to TN_4) revealed a crystalline Ti peak corresponding to the metallic Ti substrate.[20] L_1 to L_4 and D_1 to D_4 samples show similar types of XRD pattern as that of the TN_2 (not shown here).

The PL emission spectra of the samples (TN_1 to TN_4) as shown in Figure 3b were obtained for the excitation of 300 nm. Two principal emission peaks are identified for all the four cases, corresponding to (i) band-edge emission (BEE) peak in the wavelength between 393.97 to 374.92 nm (in UV region) and (ii) the peak near 467 nm, originated from oxygen vacancies (V_o).[10] The BEE peak of TN_1 to TN_4 is significantly shifted toward higher to lower wavelength side (394 to 375 nm/3.15 to 3.31 eV) indicating more stoichiometric TiO_2 nanotube formation with increasing H_2O content in the electrolyte (shown in inset of Figure 3b). The BEE peak shift is highest for TN_4 compared to that of the others. To the contrary, no significant shift is observed for the V_o-related peaks for all the four samples. Intensity of the V_o peaks compared to the BEE peaks [i.e., $I_{(Vo)}/I_{(BEE)}$] is increased with lowering of the H_2O content in the electrolyte due to the existence of higher amount of V_o-related defects. TN_1, being the most reduced one, exhibits the highest intensity V_o peak (2.66 eV) owing to the oxygen vacancy induced trap-assisted recombination [i.e., $I_{(Vo)}/I_{(BEE)}$ is maximum].[21] TN_4, being anodized in aqueous electrolyte, exhibited most stoichiometric oxide growth with negligible defect (V_o) states as manifested from the high-intensity BEE peak (with highest band gap energy at 3.31 eV) [i.e., $I_{(Vo)}/I_{(BEE)}$ is the minimum]. Analysis of PL spectra indicates that the amount of V_o was significantly higher in case of the TiO_2, grown by using electrolyte with lower H_2O content, than those with higher H_2O content. On the other hand, TiO_2 nanotube array with variable tube lengths (L_1 to L_4) and variable wall thicknesses (D_1 to D_4) exhibited negligible variation in $I_{(Vo)}/I_{(BEE)}$ value compared to that of the TN_2, and this phenomenon confirmed that the major variations of the relative peak intensity [$I_{(Vo)}/I_{(BEE)}$] and shifting of the BEE peaks were originated from the variation of the V_O in the TiO_2 nanotube array and were not due to variations in the structural parameters like length and wall thickness.

Electrochemical Capacitance Voltage Measurement. Approximate carrier density (N_D) of all the stoichiometrically varied (or variable V_O) TiO_2 nanotubes (TN_1–TN_4) was estimated by Mott–Schottky plot ($1/C^2$ vs potential). The slopes of the linear parts of the curves in the Mott–Schottky plot were found to be positive, implying that the samples were n-type semiconductors as shown in Figure 4. Capacitance measurements were conducted according to the following equation (eq 2)

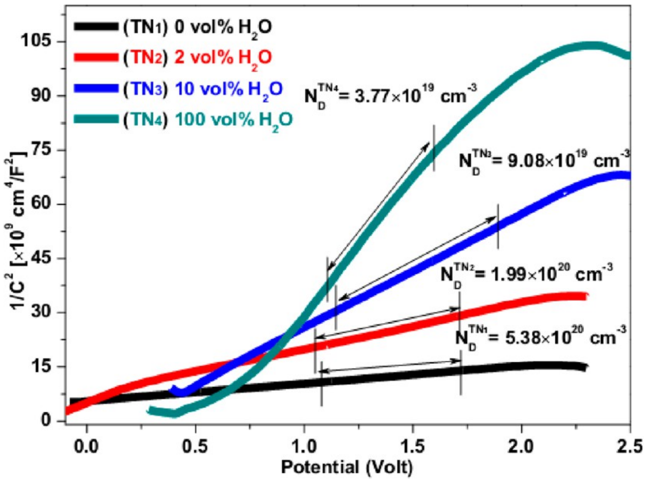

Figure 4. Mott–Schottky plot for stoichiometrically varried different TiO_2 nanotubes (TN_1 to TN_4) in 0.1 M NaOH electrolyte, recorded at a constant frequency of 0.138 kHz.

$$\frac{1}{C^2} = \frac{2}{N_D e\, \varepsilon_0 \varepsilon_r}\left[(V - V_{FB}) - \frac{kT}{e}\right] \tag{2}$$

where C is the space charge capacitance in the semiconductor, N_D is the carrier density, e is the electronic charge, ε_0 is the permittivity of the vacuum, ε_r is the relative permittivity of the semiconductor, V is the applied potential, V_{FB} is the flat band potential, k is the Boltzmann constant, and T is the temperature.

Electrical poperty (or donor density level) of TiO_2 nanotubes was obtained by electrochemical measurement of the space charge layer capacitance following the relationship (eq 3)[22]

$$N_D = \left(\frac{2}{e\, \varepsilon_0 \varepsilon_r}\right)\left[\frac{d\left(\frac{1}{C^2}\right)}{dV}\right]^{-1} \tag{3}$$

where $\varepsilon_0 = 8.85 \times 10^{-14}$ F/cm^{-1}, $e = 1.6 \times 10^{-19}$ C, and ε_r of the anatase TiO_2 ($\varepsilon_r = 48$).[4] As revealed from the C–V plot in Figure 4, all of the four TiO_2 nanotubes (TN_1 to TN_4) showed n-type conductivity (due to positive slope) with carrier density of $N_D(TN_1) = 5.38 \times 10^{20}$ cm^{-3}, $N_D(TN_2) = 1.99 \times 10^{20}$ cm^{-3}, $N_D(TN_3) = 9.08 \times 10^{19}$ cm^{-3}, and $N_D(TN_4) = 3.77 \times 10^{19}$ cm^{-3}.

A negligible but contunious decreasing trend of the carrier density (N_D) from 9.08×10^{19} cm^{-3} to 5.16×10^{19} cm^{-3} was observed with increase in anodization time (i.e., increase in tube length). The C–V measurement was also performed for the D_1–D_4 samples, and a decreasing nature of carrier density (N_D) from 9.08×10^{19} cm^{-3} to 7.92×10^{19} cm^{-3} was observed from D_1 to D_4.

Sensor Study. Alcohol (methanol, ethanol, and 2-propanol) sensing was performed for the anodically grown TiO_2 nanotube array (TN_1 to TN_4), targeting the concentration and temperature ranges of 10–1000 ppm and 27 to 250 °C, respectively. For all of the four sensor devices, the response magnitude was found to be in the order of methanol > ethanol > 2-propanol at all the temperatures. The TN_2 was found to be the most promising sensor layer compared to the others (i.e., TN_1, TN_3, and TN_4). Sensor study was also performed using L_1 to L_4 and D_1 to D_4 samples to investigate the influence of other structural parameters like tube length and tube wall thickness on the alcohol sensing. Keeping the similarity in the trend in view, only the results for methanol sensing are furnished herein.

Sensing Performance of TiO_2 Nanotubes with Variable V_O. Figure 5a represents the sensor response as the function of temperatures (TN_1 to TN_4) in the temperature range of 27–250 °C with exposure to 1000 ppm alcohol (methanol, ethanol, and 2-propanol). The onset of sensing for TN_1, TN_2, TN_3 and TN_4 sample was noted at 100, 27, 50, and 100 °C as shown in Figure 5a–d, respectively. Optimum sensing performance for TN_2 to TN_4 was observed at 150 °C and for TN_1 at 200 °C. Maximum response for TN_1 to TN_4 was recorded at ~77.5, 95.5, 86.4, and 67% for 1000 ppm methanol at their optimum operating temperature as shown in Figure 5a–d. It is evident that TN_2 exhibits the best sensing performance in the set, with the highest response magnitude for the entire temperature range (Figure 5b). Apart from that, TN_2 also offers efficient room temperature (27 °C) alcohol sensing with 60.2, 45.7, and 35.7% response magnitude for exposure in 1000 ppm methanol, ethanol, and 2-propanol, respectively.

The dynamic range (10–1000 ppm) of alcohol detection for different sensors was studied at the corresponding optimum operating temperatures (200 °C for TN_1 and 150 °C for TN_2, TN_3, and TN_4) as shown in Figure 6a–d. The sensor response increases monotonically with increase in the alcohol concentrations up to 700 ppm. Further increase in the concentrations (>700 ppm) does not exhibit any effective increment in response magnitude. Below 10 ppm, the sensor does not show any perceptible response toward any alcohol vapor.

The transient response characteristics further reveal lowest difference between each of the alcohols in the case of TN_2. Generally, response magnitude of different alcohols strongly depends on two factors: (i) molecular size/molecular weight of the alcohols in gaseous phase[23−25] and (ii) oxidation potential of alcohols in gaseous phase.[24] Increase in the carbon chain length

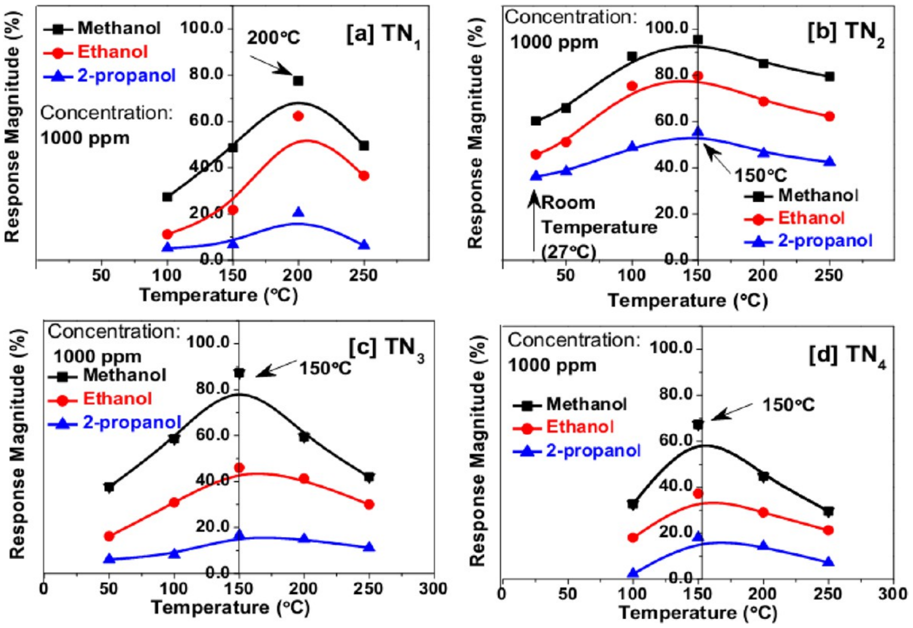

Figure 5. Sensing performance of TiO_2 nanotube array (TN_1 to TN_4) with percentage response magnitude as a function of temperatures (27−250 °C) with exposure to1000 ppm alcohol. (a) TN_1, (b) TN_2, (c) TN_3, and (d) TN_4.

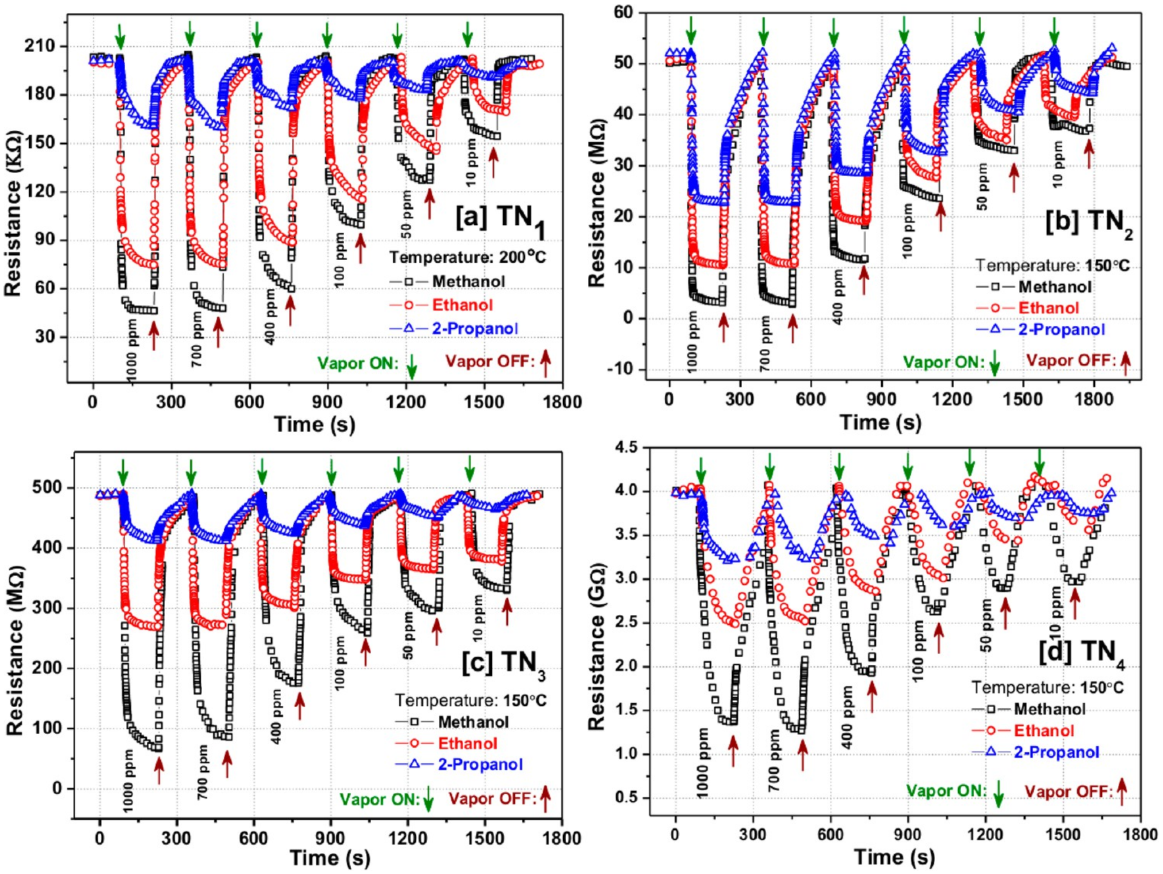

Figure 6. Transient response characteristics of TiO_2 nanotubes-based sensors in the alcohol concentration range of 10−1000 ppm at the respective optimum operating temperature. (a) TN_1, (b) TN_2, (c) TN_3, and (d) TN_4.

(2-propanol > ethanol > methanol) increases the H^+ donation capability of the alcohols (in gaseous phase), leading to the easy oxidation of alcohols.[26−29] This phenomenon is more favorable for 2-propanol compared to that of the methanol. However, in the present study, higher rate of surface adsorption appears to be the more dominant factor than that of the oxidation of the adsorbed species possibly due to the low operating temperature due to the smaller molecular size/weight.[24] Rate of surface adsorption increases in the order of methanol > ethanol >2-propanol, which may be responsible for the observed order of the response magnitude in the present case.

Figure 7 shows the transient characteristics of TN_2 (single pulse) for the response time of 7, 11, and 12 s as well as recovery time of 107, 117, and 121 s for 1000 ppm methanol, ethanol, and 2-propanol, respectively, at 150 °C. All the sensors show the decreasing trends of the response time with increase in the alcohol concentrations owing to adequate availability of the target molecules that enhances the surface coverage leading toward higher rate of surface adsorption. With lower surface coverage of the target molecules at the lower parts per million level, rate of desorption becomes faster just after cutting off the alcohol pulse, which might be the reason for the faster recovery.[30,31]

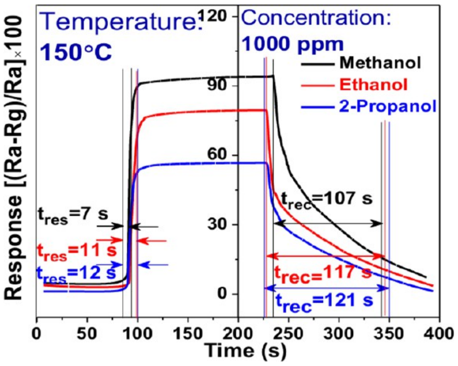

Figure 7. Transient response of TN_2 (single pulse) at 150 °C in 1000 ppm of alcohols.

Sensing Performance of TiO_2 Nanotubes with Variable Tube Lengths. Following the determination of suitable stoichiometry (TN_2), the influence of other structural parameters (like length and wall thickness) on the alcohol-sensing performance was investigated for the L_1, L_2, L_3, and L_4 sensors with the corresponding tube lengths of 1.25, 1.65, 1.95, and 2.4 μm for the methanol detection (10−1000 ppm) within the temperature range from 50 to 200 °C. Figure 8a shows that all the sensors offer the maximum response at 150 °C. Response magnitude as a function of methanol concentrations (Figure 8a, inset) reveals the increasing nature of sensor response with methanol concentrations up to 700 ppm (and saturation after 700 ppm). It is evident from the plot that variation in the tube length hardly influences the sensing performance (95 ± 1% at 150 °C in 1000 ppm methanol). It may also be seen that the sensor (L_1 to L_4) offers almost similar sensing characteristics to that of TN_2. The detailed transient responses of the sensors (L_1 to L_4) are represented in Figure 8b. Evidently, the response characteristics of the four sensors are almost comparable.

Sensing Performance of TiO_2 Nanotubes with Variable Tube Wall Thicknesses. The alcohol (methanol)-sensing performance was studied for TiO_2 nanotubes with variable tube wall thickness (D_1 to D_4) with optimum stoichiometry and length as shown in Figure 9a. The response magnitude as a function of temperature shows the maximum response at 150 °C with significant variations of response characteristics for different sample (D_1 to D_4). However, the response magnitude reveals an increasing tendency from D_1 to D_3 (D_1: 95, D_2: 96.3, D_3: 97.4%) and decreasing tendency for D_4 (90%) at 150 °C in 1000 ppm methanol. The similar trend is maintained throughout the temperature range (50−200 °C). Baseline resistance of the four sensor devices (D_1 to D_4) increases monotonically from 50 to 270 MΩ for the D_1 to D_4, as shown in Figure 9b.

Selectivity and Stability Study. Selectivity study of the optimized (stoichiometry, length, and wall thickness) sensor device (D_3) toward alcohols (methanol, ethanol, and 2-propanol) was tested in the presence of other interfering species like acetone, 2-butanone benzene, xylene, and toluene, and the result is shown in Figure 10a. Selectivity was tested for 100 ppm concentration of the volatile organic compounds at the operating temperature of 150 °C. The device with D_3 sensor layer offered the most promising selectivity for all the alcohols compared to that of the ketones and the aromatic compounds as evident from Figure 10a. Long-term stability of the sensor (D_3) was tested in exposure of air and in 1000 ppm methanol for 15 d at 150 °C as shown in Figure 10b. The maximum deviation of ±6.5% and ±17.6% was recorded for the measured resistance at 150 °C in air and in 1000 ppm methanol, respectively. TiO_2 nanotube samples were annealed at 300 °C for 4 h for developing the mechanical strength, whereas the alcohol sensing was performed below 250 °C. So, no significant variations in the nanostructure were expected even after long-term (∼14−15 weeks) alcohol sensing.

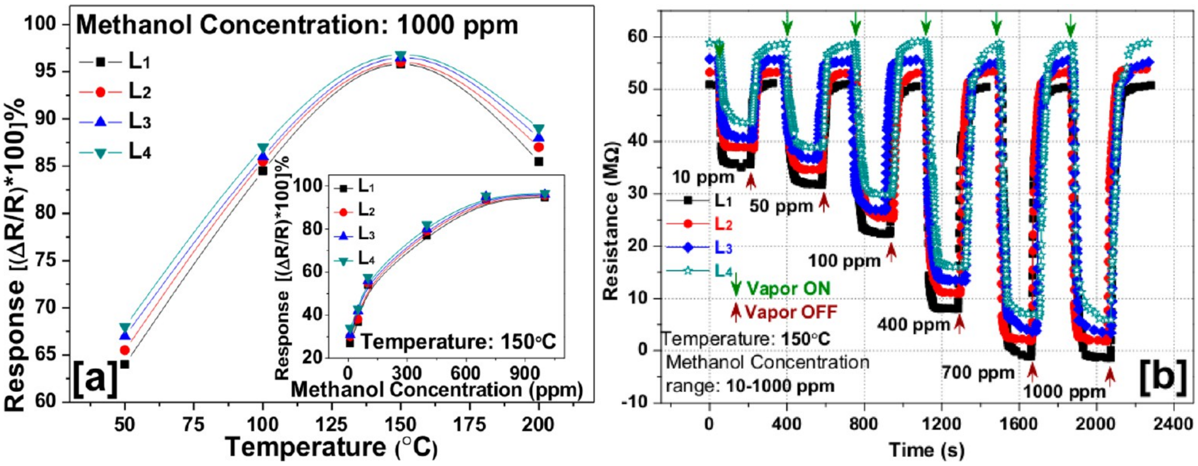

Figure 8. Methanol-sensing performance of TiO_2 nanotube array with variable tube lengths (L_1 to L_4). (a) Response magnitude as a function of temperature (50−200 °C). (inset) Response magnitude as a function of methanol concentration (10−1000 ppm). (b) Transient response characteristics of L_1 to L_4 sensors in the methanol concentration range of 10−1000 ppm at the optimum temperature (150 °C).

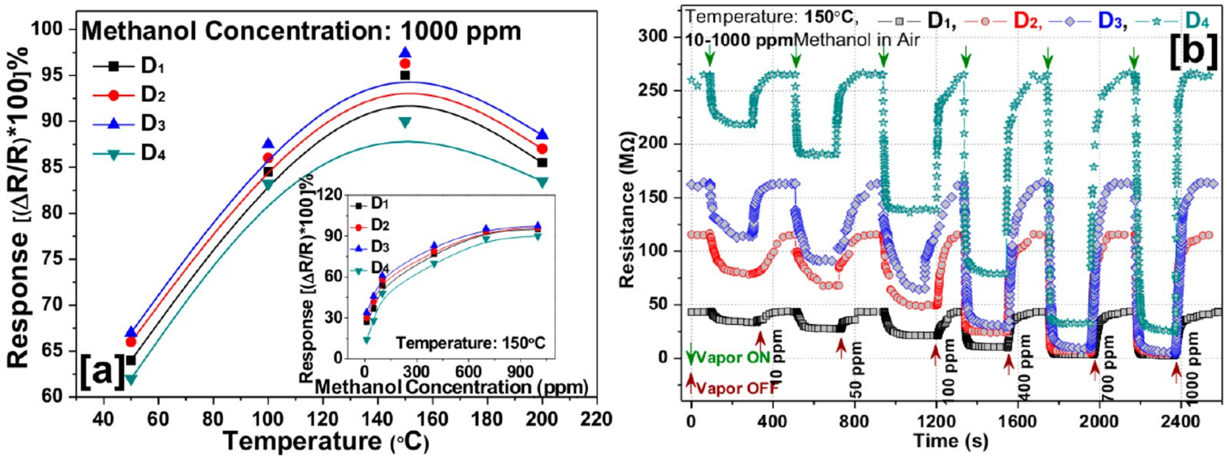

Figure 9. Methanol-sensing performance of TiO_2 nanotube array with variable tube wall thicknesses (D_1 to D_4). (a) Response magnitude as a function of temperature (50−200 °C). (inset) Response magnitude as a function of methanol concentration (10−1000 ppm). (b) Transient response characteristics of D_1 to D_4 sensors in the methanol concentration range of 10−1000 ppm at 150 °C.

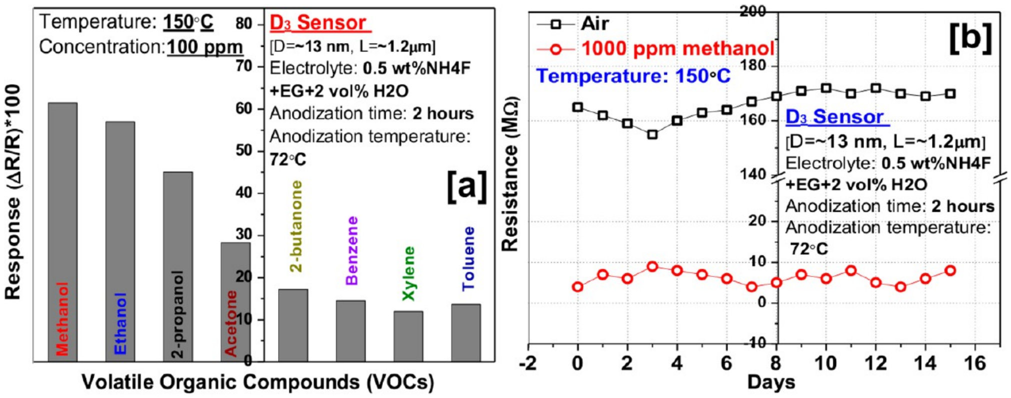

Figure 10. (a) Selectivity and (b) long-term stability performance of the TiO_2 nanotube-based sensor (D_3) with ∼13 nm of wall thickness (D) and 1.2 μm of tube length, synthesized by using 2 vol % H_2O in mixed electrolyte (0.5 wt % NH_4F + EG).

To authenticate the same, FESEM and XRD studies of the film (after sensing) were performed, and no significant changes (with respect to the film before sensing) were observed.

Comparison of Sensing Performances with Recent Literature. Table 2 comprehensively represents the comparison of the sensor performance parameters obtained from the most recent literature for different nanostructured materials-based sensors for efficient alcohol detection with the present work. As clearly reflected from Table 2, the developed sensor maintained a judicious balance between all the sensing parameters compared to earlier reported alcohol sensors. Present sensor offered high dynamic range, moderately low operating temperature, and sufficiently high response magnitude. Though the sensor showed apparently fast response toward all the alcohols, recovery performance of the sensor was not very promising.

Sensing Mechanism. *Role of Oxygen Vacancy.* The sensor study exhibited two distinctive improvements: (i) relatively low operating temperature for sensing and (ii) appreciably high response magnitude, which were achieved by judiciously controlling the nanotube parameters through varying the H_2O content in the electrolyte during the anodization process. In the case of TN_1, though the amount of V_o is the highest, extremely poor surface-to-volume ratio resulted into the low operating temperature compared to that of TN_2, TN_3, and TN_4.

The operating temperature and corresponding response magnitude of the semiconducting metal oxide-based gas/vapor sensor principally depend on (i) binding interaction between the target gas/vapor species and the semiconducting surface,[44] (ii) effective surface area of the nanotubes providing the available gas interaction sites,[45] (iii) dissociative adsorption of oxygen and alcohol molecules,[46,47] and (iv) required activation energy for the electronic transport (which is related to the barrier potential (qV_b) between two grains).[48] Among these parameters, (i), (iii), and (iv) directly depend on the concentrations of V_o in the semiconducting oxide. At the same time, availability of the gas interaction sites can also be enhanced by increasing the surface-to-volume ratio of the sensing layer.

V_o-related defect sites/states are the most favorable ones for the adsorption of target species (alcohols in the present case).[46,49] This is because the binding interaction between O_2 molecules and alcohol molecules is much stronger in such defect sites compared to the defect-free ones. O_2 molecules can be dissociated and chemisorbed to the oxygen vacant site (V_o) of the oxide surface with negligible activation energy, and the rate of adsorption increases with increase in operating temperature up to a certain limit [case (iii)].[46,50]

As the reducing gas/vapor comes to contact the sensing layer, it is adsorbed to the oxide surface by the dissociative adsorption process and dehydrogenated by the adsorbed oxygen species. Catalytic activity of TiO_2 enhances the dissociation possibility of the alcohols to the oxide surface.[51,52] By the effect of TiO_2 catalyst, O−H bond scission becomes faster, and alcohols can

Table 2. Comparison of Sensor Parameters of the Developed TiO_2 Nanotube-Based Alcohol Sensor with Other Sensors Reported in Recent Literature

Sl. No.	nanomaterials	target alcohol[a]	detection range (ppm)	optimum temperature (°C)	response magnitude	response time[b] (s)	recovery time[b] (s)	ref
1	Nb-doped TiO_2 nanorods	Et	400	550	Ra/Rg = 12	3	79	32
2	surface-coarsened Ag–TiO_2 nanobelts	Et	500	200	Ra/Rg = 46.15	1	2	31
3	nanocrystalline La–Pb–Fe–O perovskite	Mt	400	230	Rg/Ra = 146.6	40	75	33
4	CdS-doped SnO_2 thick film	Mt	5000	200	$(\Delta R/\text{Ra})*100$ = 70%	40	110	34
5	nanostructured MoO_3:ZnO thin films	Et	500	300	Gg/Ga = 171	75	70	35
6	screen-printed WO_3 thick films	Et	50	400	(Ra/Rg)*100 = 1424%	10	45	36
7	SnO_2 carbon nanotubes	Mt	30	RT	$\Delta R/\Delta C = 13 \times 10^{-2}$	<60	<60	37
8	one-dimensional zinc oxide nanorods	Et	12.5–500	310	Ra/Rg = 2.3	16	120	38
9	Au-modified ZnO nanowires	Et	100	300	Ra/Rg = 89.5	5	20	39
10	TiO_2 core/shell nanorods	Et	10–500	180	Ra/Rg = 11.5	<40	<10	40
11	Ag nanoparticle-modified TiO_2 nanosphere	Et	50–10000	350	Ra/Rg = 2	5	49	30
12	CeO_2/TiO_2 core/shell nanorods	Et	10–1000	320	Ra/Rg = 7.75	<45	<45	41
13	Nb-doped TiO_2 nanoparticle	Et	10–500	350	Ra/Rg = 41.4	9	300	42
14	ZnO nanorods	Mt	950	150	$(\Delta R/\text{Ra})*100$ = 90%	8–19	39–55	43
16	TiO_2 nanotube array	Mt	10–1000	150	$(\Delta R/\text{Ra})*100$ = 94%	7	107	present work
17	TiO_2 nanotube array	Et	10–1000	150	$(\Delta R/R)*100$ = 73%	11	117	presnt work

[a] Et: ethanol, Mt: methanol, RT: room temperature. [b] The response time and recovery time of the sensor were calculated as the time taken by the sensor signal to reach 90% (or to fall at 10%) of (from) its saturation value upon exposure (or removal) of ethanol vapor pulse.

easily be dissociated [case (iii)] and dehydrogenated into different alkoxy fragments, namely, $[CH_3O]^-$ for methanol, $[CH_3CH_2O]^-$ for ethanol, and $[CH_3CH_3CHO]^-$ for 2-propanol, and hydroxyl groups.[52,53] All the species are adsorbed to the TiO_2 nanotube surface occupying two active defect sites (originated from V_o) according to the following reaction (eq 4).[46,54] Because of the capture of free electron to the oxide surface, sensor resistance decreases effectively.

$$ROH_{(vapor)} + O^-_{(ads)} \rightarrow [RO]^-_{(ads)} + OH^-_{(ads)} \qquad (4)$$

where R represents the alkoxy group.

Subsequently, the adsorbed alkoxy fragments recombine with the adsorbed hydroxyl ions and form the molecular alcohols releasing a free defect site following the reversible process as[46]

$$[RO]^-_{(ads)} + OH^-_{(ads)} \rightarrow ROH_{(vapor)} + O^-_{(ads)} \qquad (5)$$

Two adsorbed hydroxyl groups then react with each other and release H_2O and a free electron (offering a free defect site) following the reaction[46]

$$OH^-_{(ads)} + OH^-_{(ads)} \rightarrow H_2O + O^-_{(ads)} + e^- \qquad (6)$$

The adsorbed alcohol (ROH) molecules can also be directly oxidized or dehydrogenated (eq 7) by the surface-adsorbed oxygen and generate final product as the combination of CO_2 and H_2O at relatively elevated temperature by releasing free electrons (offering free defect sites) to the oxide surface that effectively reduces the sensor resistance of the n-type TiO_2 nanotube array as[55]

$$ROH_{(ads)} + O^-_{(ads)} \rightarrow CO_{2(gas)} + H_2O_{(gas)} + e^- \qquad (7)$$

Therefore, the aforesaid possibilities confirm that the alcohol-sensing performance strongly depends on the availability of the V_o-originated defect sites (eqs 4–7). At the low temperature, adsorption of the alkoxy group on the nanotube surface strongly depends on the availability of the oxygen vacant sites and the surface coverage of the alkoxy groups.[46,50] At any particular alcohol concentration, when surface coverage of the alkoxy groups is almost constant, response magnitude of a sensor is principally dominated by the availability of the free oxygen vacant sites (V_o).

With increase in the concentration of V_o (more reduced TiO_2), free electron concentration increases leading to the higher electrical conductivity (σ) with reduced barrier potential. So, the required activation energy can be modulated by controlling the concentration of V_o (through amount of H_2O in electrolyte).[48] The ECV study (Figure 4) confirmed this. Despite the activation energy of electron transport being minimum for TN_1 ($TN_1 < TN_2 < TN_3 < TN_4$), the overall response magnitude of TN_1 is not very promising owing to its relatively poor surface-to-volume ratio.

Role of Surface-to-Volume Ratio. In the present case, very low (i.e., TN_1) and very high (i.e., TN_4) H_2O content in the electrolyte resulted in relatively poor surface-to-volume ratio [case (ii)]. The TN_1 sample showed almost no wall separations, and the TN_4 offered maximum wall separations between neighboring nanotubes. Eventually, both TN_1 and TN_4 suffer from poor surface-to-volume ratio of the oxide surface resulting in poor alcohol-sensing performance in terms of the operating temperature and response magnitude.

To calculate the surface-to-volume ratio of a single TiO_2 nanotube, rectangular cuboids can be considered around a single

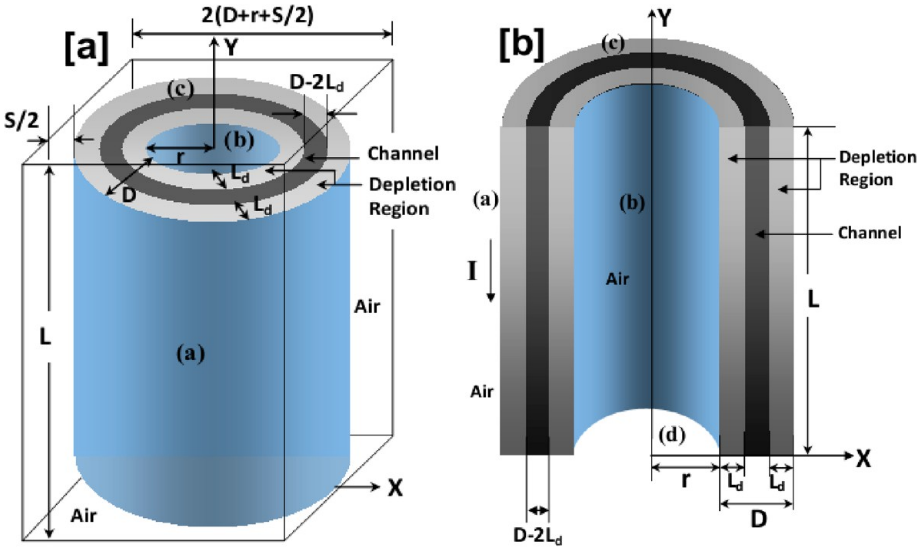

Figure 11. Schematic of an individual TiO_2 nanotube indicating the dimensions and planes. (a) Complete view of a nanotube. (b) Cross-sectional view of a nanotube (L_d is the width of depletion layer).

nanotube as depicted in Figure 11a,b. Let the inner diameter, wall thickness, tube length, and wall separation of the nanotube be designated as $2r$, D, L, and S, respectively. If the nanotube array consists of n number of nanotubes, surface-to-volume (SVR) of the sensing layer can be represented as

$$\mathrm{SVR} = \frac{[2\pi rL + 2\pi(r + D)L + \pi(r + D)^2] \times n}{4 \times \left(r + D + \frac{S}{2}\right)^2 \times L \times n} \tag{8}$$

As the area of the top surface (c) and bottom surface (d) of the nanotube are negligibly small compared to the outer (a) and inner (b) wall surface area, according to Figure 11a,b, $\pi(r + D)^2$ can be neglected, and the simplified surface-to-volume ratio can be represented by eq 9, which is independent of the length (L) and number (n) of the nanotubes. Hence, surface-to-volume ratio is expressed as

$$\mathrm{SVR} = \frac{2\pi r + \pi D}{2 \times \left(r + D + \frac{S}{2}\right)^2} \tag{9}$$

According to the structural configuration of TN_1 (shown in Figure 1A(a)), the outer wall surface area (a) can be neglected due to the negligible separation between the walls. So, the lowest value of surface-to-volume ratio (SVR) is obtained for TN_1 as

$$\mathrm{SVR} = \frac{\pi r}{2 \times \left(r + D + \frac{S}{2}\right)^2} \quad (\text{for } TN_1) \tag{10}$$

As TN_2 consists of both the wall-connected and wall-separated structures, outer surface of the nanotubes is considered partially, and surface-to-volume ratio value is higher than that of TN_1 and lower than that of TN_3 and TN_4. In the case of TN_3 and TN_4 samples, significant change is observed in the case of wall separations (S) (Figure 1A(c),(d)) compared to the corresponding changes in r and D. According to eq 12, higher value of S will decrease the surface-to-volume ratio in the case of TN_4 (compared to TN_3). Then, four different nanotube structures can be represented as $TN_1 < TN_2 < TN_4 < TN_3$ in the order of surface-to-volume ratio.

Although, TN_3 offers the highest surface-to-volume ratio compared to other nanotubes, it does not exhibit the best sensing performance due to the lower concentrations of V_O. The TN_2 sample, owing to the availability of V_O and promising surface-to-volume ratio, offers the best sensing performance at relatively low temperatures (even at room temperature). To the contrary, the TN_1 sample, despite having a large amount of V_O sites, suffers from inferior surface-to-volume ratio (almost no nanotube was formed). At the same time, TN_4, with relatively high effective surface area, is unable to show promising alcohol sensing at relatively low temperature due to the absence of adequate V_O sites. Therefore, the processing of the TiO_2 nanotubes warrants the best combination of V_O and surface-to-volume ratio of the nanotube structures (as achieved in the case of TN_2) to offer the promising alcohol-sensing performance.

Role of Channel Formation. Though the above mechanism largely demonstrates the efficiency of alcohol-sensing performance for the TiO_2 nanotube-based (TN_2) sensors, it cannot explain the effect of the tube length (L) and wall thickness (D) variations on the alcohol-sensing performance. To explain the effect of all the structural parameters (i.e., $2r$, D, L, N_D), the channel formation mechanism has been invoked.[56,57]

In this model, an individual TiO_2 nanotube is considered as a single resistance (R) with length L and cross sectional area A. The tube is assumed to have an average free electron density N_D and mobility μ_n. The tube resistance can be represented as

$$R = \frac{1}{qN_D\mu_n} \times \frac{L}{A} \tag{11}$$

In air ambient, inner and outer surface of the nanotube is depleted partially due to adsorption of the oxygen species (O^-, O^{2-}, etc.) on the nanotube surface. The conducting channels between the surfaces (inner and outer) have the dimension of $D - 2L_d$, where L_d is the thickness of depleted region as shown in Figure 11a,b.[58,59] Considering the conducting channel formation possibility, eq 11 can be expressed as

$$R_{(\mathrm{air})} = \frac{1}{qN_D\mu_n} \times \frac{L}{\pi(D + 2r) \times (D - 2L_d)}$$

$$\text{where} \quad L_d \equiv \sqrt{\frac{\varepsilon_0\varepsilon_r kT}{q^2(N_D - n_a)}} \tag{12}$$

$$R_{(\mathrm{air})} = \frac{1}{qN_{\mathrm{D}}\mu_{\mathrm{n}}} \times \frac{L}{\pi(D + 2r) \times \left(D - 2\sqrt{\frac{\varepsilon_0\varepsilon_r kT}{q^2(N_{\mathrm{D}} - n_{\mathrm{a}})}}\right)} \tag{13}$$

where n_{a} is the captured electron due to surface adsorption of oxygen species.

In ambient reducing vapor (like alcohols), a fraction of the captured electrons is released (n_{g}) to the nanotube surface, thereby increasing the channel width ($D - 2L_{\mathrm{d}}$) and lowering the sensor resistance as shown in eq 14.

$$R_{(\mathrm{alcohol})} = \frac{1}{qN_{\mathrm{D}}\mu_{\mathrm{n}}} \times \frac{L}{\pi(D + 2r) \times \left(D - 2\sqrt{\frac{\varepsilon_0\varepsilon_r kT}{q^2(N_{\mathrm{D}} - n_{\mathrm{a}} + n_{\mathrm{g}})}}\right)} \tag{14}$$

Response magnitude of the nanotube-based planar sensor can therefore be expressed as

$$\mathrm{RM} = \frac{R_{(\mathrm{air})} - R_{(\mathrm{alcohol})}}{R_{(\mathrm{air})}} = 1 - \frac{D - 2\sqrt{\frac{\varepsilon_0\varepsilon_r kT}{q^2(N_{\mathrm{D}} - n_{\mathrm{a}})}}}{D - 2\sqrt{\frac{\varepsilon_0\varepsilon_r kT}{q^2(N_{\mathrm{D}} - n_{\mathrm{a}} + n_{\mathrm{g}})}}} \tag{15}$$

Equation 13 represents the baseline resistance of the sensor. With increase in tube length (L) and decrease in tube wall thickness (D), baseline resistance of the sensor ($R_{(\mathrm{air})}$) increases as evidenced from the experimental results as shown in Figures 8b and 9b, respectively. The rapid decrement of the sensor resistance ($R_{(\mathrm{air})}$) with increase in V_{O} content (or increase in carrier density, N_{D}) can be correlated with eq 14. Moreover, the expression of response magnitude in eq 15 confirms that there is limited effect of the tube length variations on the sensing performance of the sensor, which also agrees well with the experimental findings (Figure 8). On the other hand, sensing performance strongly depends on nanotube wall thickness (D), and response magnitude (RM) is found to increase with decrease in the tube wall thickness (according to eq 15). This is also in line with the experimental results as presented in Figure 9.

CONCLUSION

The present work concerns the systematic approach to establish the most favorable combination of three pivotal structural parameters of the nanotube structure, namely, (i) stoichiometry/oxygen vacancies, (ii) lengths, and (iii) wall thicknesses of electrochemically grown TiO_2 nanotubes, with an aim to achieve efficient alcohol-sensing performance. The stoichiometry of the nanotubes (V_{o}) was optimized by varying the H_2O content (0%, 2%, 5%, 10%, and 100% by vol) in the EG- and NH_4F-based mixed electrolyte. As a result, four distinctly different nanoforms were achieved. It is revealed that neither of the structural parameters, that is, (i) the lowest surface-to-volume ratio and the highest oxygen vacancies (most non-stoichiometric) and (ii) the highest surface-to-volume ratio with the lowest oxygen vacancies (most stoichiometric), offer promising sensing performance. The best optimization of these two parameters in the case of TN_2 offered the most promising alcohol-sensing performance with superior response magnitude along with appreciably fast response time. For this particular stoichiometry, the lengths and wall thicknesses of the nanotubes were varied (sequentially), by varying the anodization time and temperatures, respectively. While the length variation hardly influenced the sensing performance, a typical wall thickness of ~13 nm was found to be the optimum for achieving promising response magnitude.

AUTHOR INFORMATION

Corresponding Author

*E-mail: pb_etc_besu@yahoo.com.

Notes

The authors declare no competing financial interest.

ACKNOWLEDGMENTS

This work was supported by Indian National Science Academy (INSA; Sanction Letter No. SP/YSP/81/2013/735). The authors sincerely acknowledge Dr. M. Ray, School of Materials Science and Engineering, IIEST, Howrah 711 103, India, for providing the facility of PL spectroscopy. A.H. gratefully acknowledges the Department of Science and Technology (DST), Govt. of India, for the INSPIRE Fellowship for pursuing his Ph.D. program. B.B. and K.D. thankfully acknowledge COE, TEQIP−II, IIEST, Shibpur, for their fellowship for pursuing Ph.D. program.

REFERENCES

(1) Hazra, A.; Bhowmik, B.; Dutta, K.; Manjuladevi, V.; Gupta, R. K.; Chattopadhyay, P. P.; Bhattacharyya, P. Formation Mechanism of Anodically Grown Free-standing TiO_2 Nanotube Array Under the Influence of Mixed Electrolytes. *Sci. Adv. Mater.* **2014**, *6*, 714−719.

(2) Hazra, A.; Bhattacharyya, P. Tailoring of the Gas Sensing Performance of TiO_2 Nanotubes by 1-D Vertical Electron Transport Technique. *IEEE Trans. Electron Devices* **2014**, *61*, 3483−3489.

(3) Kim, J. Y.; Noh, J. H.; Zhu, K.; Halverson, A. F.; Neale, N. R.; Park, S.; Hong, K. S.; Frank, A. J. General Strategy for Fabricating Transparent TiO_2 Nanotube Arrays for Dye-sensitized Photoelectrodes: Illumination Geometry and Transport Properties. *ACS Nano* **2011**, *5*, 2647−2656.

(4) Lu, H. F.; Li, F.; Liu, G.; Chen, Z.-G.; Wang, D.-W.; Fang, H.-T.; Lu, G. Q.; Jiang, Z. H.; Cheng, H.-M. Amorphous TiO_2 Nanotube Arrays for Low-temperature Oxygen Sensors. *Nanotechnology* **2008**, *19*, 405504.

(5) Kwon, Y.; Kim, H.; Lee, S.; Chin, I.; Seong, T.; Lee, W.; Lee, C. Enhanced Ethanol Sensing Properties of TiO_2 Nanotube Sensors. *Sens. Actuators, B* **2012**, *173*, 441−446.

(6) Perillo, P. M.; Rodríguez, D. F. The Gas Sensing Properties at Room Temperature of TiO_2 Nanotubes by Anodization. *Sens. Actuators, B* **2012**, *171−172*, 639−643.

(7) Kılınç, N.; Şennik, E.; Öztürk, Z. Z. Fabrication of TiO_2 Nanotubes by Anodization of Ti Thin Films for VOC Sensing. *Thin Solid Films* **2011**, *520*, 953−958.

(8) Kar, P.; Pandey, A.; Greer, J. J.; Shankar, K. Ultrahigh Sensitivity Assays for Human Cardiac Troponin I using TiO_2 Nanotube Arrays. *Lab Chip* **2012**, *12*, 821−828.

(9) Yoriya, S.; Prakasam, H. E.; Varghese, O. K.; Shankar, K.; Paulose, M.; Mor, G. K. Initial Studies on the Hydrogen Gas Sensing Properties of Highly-Ordered High Aspect Ratio TiO_2 nanotube-arrays 20 to 222 μm in Length. *Sens. Lett.* **2006**, *4*, 334−339.

(10) Hazra, A.; Dutta, K.; Bhowmik, B.; Manjuladevi, V.; Gupta, R. K.; Chattopadhyay, P. P.; Bhattacharyya, P. Structural and Optical Characterizations of Electrochemically Grown Connected and Free Standing TiO_2 Nanotube Array. *J. Electron. Mater.* **2014**, *43*, 3229−3235.

(11) Hazra, A.; Dutta, K.; Bhowmik, B.; Chattopadhyay, P. P.; Bhattacharyya, P. Room Temperature Alcohol Sensing by Stoichiometry Controlled TiO_2 Nanotube Array. *Appl. Phys. Lett.* **2014**, *105*, 081604.

(12) Yanga, H.; Pan, C. Diameter-Controlled Growth of TiO_2 Nanotube Arrays by Anodization and its Photoelectric Property. *J. Alloys Compd.* **2010**, *492*, L33−L35.

(13) Roy, P.; Berger, S.; Schmuki, P. TiO_2 Nanotubes: Synthesis and Applications. *Angew. Chem., Int. Ed.* **2011**, *50*, 2904−2939.

(14) Yang, M.; Liu, W.; Sun, J.-L.; Zhu, J.-L. High Magnetic Field Annealing Effect on Visible Photoluminescence Enhancement of TiO_2 Nanotube Arrays. *Appl. Phys. Lett.* **2012**, *100*, 043106.

(15) Berger, S.; Kunze, J.; Schmuki, P.; Valota, A. T.; Leclere, D. J.; Skeldon, P.; Thompson, G. E. Influence of Water Content on the Growth of Anodic TiO_2 Nanotubes in Fluoride-Containing Ethylene Glycol Electrolytes. *J. Electrochem. Soc.* **2010**, *157*, C18−C23.

(16) Shankar, K.; Mor, G. K.; Prakasam, H. E.; Yoriya, S.; Paulose, M.; Varghese, O. K.; Grimes, C. A. Highly-ordered TiO_2 nanotube arrays up to 220 μm in length: use in water photoelectrolysis and dye-sensitized solar cells. *Nanotechnology* **2007**, *18*, 065707.

(17) Chen, C.-C.; Chung, H.-W.; Chen, C.-H.; Lu, H.-P.; Lan, C.-M.; Chen, S.-F.; Luo, L.; Hung, C.-S.; Diau, E. W-G. Fabrication and Characterization of Anodic Titanium Oxide Nanotube Arrays of Controlled Length for Highly Efficient Dye-Sensitized Solar Cells. *J. Phys. Chem. C* **2008**, *112*, 19151−19157.

(18) Chen, J.; Lin, J.; Chen, X. Self-Assembled TiO_2 Nanotube Arrays with U-Shaped Profile by Controlling Anodization Temperature. *J. Nanomater.* **2010**, No. 753253−4.

(19) Yin, H.; Liu, H.; Shen, W.-Z. The Large Diameter and Fast Growth of Self-Organized TiO_2 Nanotube Arrays Achieved via Electrochemical Anodization. *Nanotechnology* **2010**, *21*, 035601.

(20) Macak, J. M.; Tsuchiya, H.; Ghicov, A.; Yasuda, K.; Hahn, R.; Bauer, S.; Schmuki, P. TiO_2 Nanotubes: Self-organized Electrochemical Formation, Properties and Applications. *Curr. Opin. Solid State Mater. Sci.* **2007**, *11*, 3−18.

(21) Wu, F.; Hu, X.; Fan, J.; Liu, E.; Sun, T.; Kang, L.; Hou, W.; Zhu, C.; Liu, H. Photocatalytic Activity of Ag/TiO_2 Nanotube Arrays Enhanced by Surface Plasmon Resonance and Application in Hydrogen Evolution by Water Splitting. *Plasmonics* **2013**, *8*, 501.

(22) Lu, X.; Wang, G.; Zhai, T.; Yu, M.; Gan, J.; Tong, Y.; Li, Y. Hydrogenated TiO_2 Nanotube Arrays for Supercapacitors. *Nano Lett.* **2012**, *12*, 1690−1696.

(23) Balcerzak, A.; Aleksiejuk, M.; Zhavnerko, G.; Agabekov, V. Sensing Properties of Two-component Langmuir−Blodgett Layer and its Porous Derivative in SAW Sensor for Vapors of Methanol and Ethanol. *Thin Solid Films* **2010**, *518*, 3402−3406.

(24) Kozlov, M.; McCarthy, T. J. Adsorption of Poly(vinyl alcohol) from Water to a Hydrophobic Surface: Effects of Molecular Weight, Degree of Hydrolysis, Salt, and Temperature. *Langmuir* **2004**, *20*, 9170−9176.

(25) Nabiyouni, G.; Barati, A.; Saadat, M. Surface Adsorption of Polyethylene Glycol and Polyvinyl Alcohol with Variable Molecular Weights on Zinc Oxide Nanoparticles. *Iran. J. Chem. Eng.* **2011**, *8*, 20−30.

(26) Bajpai, R.; Motayed, A.; Davydovb, A. V.; Oleshkob, V. P.; Aluri, G. S.; Bertness, K. A.; Rao, M. V.; Zaghloul, M. E. UV-Assisted Alcohol Sensing Using SnO_2 Functionalized GaN Nanowire Devices. *Sens. Actuators, B* **2012**, *171*−*172*, 499−507.

(27) Ervin, K. M.; De Turi, V. F. Anchoring the Gas-Phase Acidity Scale. *J. Phys. Chem. A* **2002**, *106*, 9947−9956.

(28) Blanksby, S. J.; Barneyellison, G. Bond Dissociation Energies of Organic Molecules. *Acc. Chem. Res.* **2003**, *36*, 255−263.

(29) Wu, W.-C.; Chuang, C.-C.; Lin, J.-L. Bonding Geometry and Reactivity of Methoxy and Ethoxy Groups Adsorbed on Powdered TiO_2. *J. Phys. Chem. B* **2000**, *104*, 8719−8724.

(30) Cheng, X.; Xu, Y.; Gao, S.; Zhao, H.; Huo, L. Ag Nanoparticles Modified TiO_2 Spherical Heterostructures with Enhanced Gas-Sensing Performance. *Sens. Actuators, B* **2011**, *155*, 716−721.

(31) Hu, P.; Du, G.; Zhou, W.; Cui, J.; Lin, J.; Liu, H.; Liu, D.; Wang, J.; Chen, S. Enhancement of Ethanol Vapor Sensing of TiO_2 Nanobelts by Surface Engineering. *ACS Appl. Mater. Interfaces* **2010**, *2*, 3263−3269.

(32) Singh, S.; Kaur, H.; Singh, V. N.; Jain, K.; Senguttuvan, T. D. Highly Sensitive and Pulse-like Response Toward Ethanol of Nb Doped TiO_2 Nanorods based Gas Sensors. *Sens. Actuators, B* **2012**, *171*−*172*, 899−906.

(33) Dorofteia, C.; Popa, P. D.; Iacomi, F. Synthesis of Nanocrystalline La−Pb−Fe−O Perovskite and Methanol-Sensing Characteristics. *Sens. Actuators, B* **2012**, *161*, 977−981.

(34) Yadava, L.; Verma, R.; Dwivedi, R. Sensing Properties of CdS-Doped Tin Oxide Thick Film Gas Sensor. *Sens. Actuators, B* **2010**, *144*, 37−42.

(35) Illyaskutty, N.; Kohler, H.; Trautmann, T.; Schwotzerc, M.; Pillai, V. P. M. Enhanced Ethanol Sensing Response from Nanostructured MoO_3:ZnO Thin Films and Their Mechanism of Sensing. *J. Mater. Chem. C* **2013**, *1*, 3976−3984.

(36) Khadayate, R. S.; Waghulde, R. B.; Wankhede, M. G.; Sali, J. V.; Patil, P. P. Ethanol Vapour Sensing Properties of Screen Printed WO_3 Thick Films. *Bull. Mater. Sci.* **2007**, *30*, 129−133.

(37) Mendozaa, F.; Hernándeza, D. M.; Makarova, V.; Febus, E.; Weinera, B. R.; Morell, G. Room Temperature Gas Sensor based on Tin Dioxide-Carbon Nanotubes Composite Films. *Sens. Actuators, B* **2014**, *190*, 227−233.

(38) Ahmad, M. Z.; Sadek, A. Z.; Latham, K.; Kita, J.; Moosd, R.; Wlodarskia, W. Chemically Synthesized One-Dimensional Zinc Oxide Nanorods for Ethanol Sensing. *Sens. Actuators, B* **2013**, *187*, 295−300.

(39) Ramgir, N. S.; Kaur, M.; Sharma, P. K.; Datta, N.; Kailasaganapathi, S.; Bhattacharya, S.; Debnath, A. K.; Aswal, D. K.; Gupta, S. K. Ethanol Sensing Properties of Pure and Au Modified ZnO Nanowires. *Sens. Actuators, B* **2013**, *187*, 313−318.

(40) Chen, Y.; Xiao, G.; Wang, T.; Zhang, F.; Ma, Y.; Gao, P.; Zhu, C.; Zhang, E.; Xu, Z.; Li, Q. α-MoO_3/TiO_2 Core/Shell Nanorods: Controlled-Synthesis and Low-Temperature Gas Sensing Properties. *Sens. Actuators, B* **2011**, *155*, 270−277.

(41) Chen, Y.-J.; Xiao, G.; Wanga, T.-S.; Zhang, F.; Maa, Y.; Gaob, P.; Zhu, C.-L.; Zhang, E.; Xu, Z.; Li, Q. Synthesis and Enhanced Gas Sensing Properties of Crystalline CeO_2/TiO_2 Core/Shell Nanorods. *Sens. Actuators, B* **2011**, *156*, 867−874.

(42) Phanichphant, S.; Liewhiran, C.; Wetchakun, K.; Wisitsoraat, A.; Tuantranon, A. Flame-Made Nb-Doped TiO_2 Ethanol and Acetone Sensors. *Sensors* **2011**, *11*, 472−484.

(43) Banerjee, N.; Roy, S.; Sarkar, C. K.; Bhattacharyya, P. High Dynamic Range Methanol Sensor based on Aligned ZnO nanorods. *IEEE Sens. J.* **2013**, *13*, 1669−1676.

(44) Wu, R.-J.; Lin, D.-J.; Yu, M.-R.; Chen, M. H.; Lai, H.-F. Ag@SnO_2 Core-shell Material Use in Fast-Response Ethanol Sensor at Room Operating Temperature. *Sens. Actuators, B* **2013**, *178*, 185−191.

(45) An, W.; Wu, X.; Zeng, X. C. Adsorption of O_2, CO_2, CO, NH_3 and NO_2 on ZnO Nanotube a Density Functional Theory Study. *J. Phys. Chem. C* **2008**, *112*, 5747−5755.

(46) Sturm, J. M.; Göbke, D.; Kuhlenbeck, H.; Döbler, J.; Reinhardt, U.; Ganduglia-Pirovano, M. V.; Sauerzand, J.; Freund, H.-J. Partial Oxidation of Methanol on Well-Ordered V_2O_5 (001)/Au(111) Thin Films. *Phys. Chem. Chem. Phys.* **2009**, *11*, 3290−3299.

(47) Lopatiuk, O.; Chernyak, L.; Osinsky, A.; Xie, J. Q. Lithium-Related States as Deep Electron Traps in ZnO. *Appl. Phys. Lett.* **2005**, *87*, 214110.

(48) Rothschild, A.; Komem, Y. The Effect of Grain Size on the Sensitivity of Nanocrystalline Metal Oxide Gas Sensor. *J. Appl. Phys.* **2004**, *95*, 63746380.

(49) Ahn, M.-W.; Park, K.-S.; Heo, J.-H.; Park, J.-G.; Kim, D.-W.; Choi, K. J.; Lee, J.-H.; Hong, S.-H. Gas Sensing Properties of Defect-Controlled ZnO-Nanowire Gas Sensor. *Appl. Phys. Lett.* **2008**, *93*, 263103.

(50) Orzol, M.; Martin, I.; Kocisek, J.; Dabkowska, I.; Langer, J.; Illenberger, E. Bond and Site Selectivity in Dissociative Electron Attachment to Gas Phase and Condensed Phase Ethanol and Trifluoroethanol. *Phys. Chem. Chem. Phys.* **2007**, *9*, 3424−3431.

(51) Yang, X.; Wang, X.; Liang, C.; Su, W.; Wang, C.; Feng, Z.; Li, C.; Qiu, J. Aerobic Oxidation of Alcohols over Au/TiO_2: An Insight on the Promotion Effect of Water on the Catalytic Activity of Au/TiO_2. *Catal. Commun.* **2008**, *9*, 2278−2281.

(52) Gazsi, A.; Schubert, G.; Bánsági, T.; Solymosi, F. Photocatalytic Decompositions of Methanol and Ethanol on Au Supported by Pure or N-doped TiO_2. *J. Photochem. Photobiol., A* **2013**, *271*, 45−55.

(53) Chen, G.; Li, S.; Jiao, F.; Yuan, Q. Catalytic Dehydration of Bioethanol to Ethylene over $TiO_2/\gamma\text{-}Al_2O_3$ Catalysts in Microchannel Reactors. *Catal. Today* **2007**, *125*, 111−119.

(54) Ibanescu, B. C.; May, O.; Monney, A.; Allan, M. Electron-Induced Chemistry of Alcohols. *Phys. Chem. Chem. Phys.* **2007**, *9*, 3163−73.

(55) Choudhary, K.; Manjuladevi, V.; Gupta, R. K.; Bhattacharyya, P.; Hazra, A.; Kumar, S. Ultrathin Films of TiO_2 Nanoparticles at Interfaces. *Langmuir* **2015**, *31*, 1385−1392.

(56) Barsan, N.; Weimar, U. Understanding the Fundamental Principles of Metal Oxide based Gas Sensors; the Example of CO Sensing with SnO_2 Sensors in the Presence of Humidity. *J. Phys.: Condens. Matter* **2003**, *15*, R813−R83.

(57) Pokhrel, S.; Simion, C. A.; Quemener, V.; Barsan, N.; Weimar, U. Investigations of Conduction Mechanism in Cr_2O_3 Gas Sensing Thick Films by AC Impedance Spectroscopy and Work Function Changes Measurements. *Sens. Actuators, B* **2008**, *133*, 78−83.

(58) Barsan, N.; Simion, C.; Heine, T.; Pokhrel, S.; Weimar, U. Modeling of Sensing and Transduction for p-type Semiconducting Metal Oxide based Gas Sensors. *J. Electroceram.* **2010**, *25*, 11−19.

(59) Hübnera, M.; Simion, C. E.; Tomescu-Stanoiu, A.; Pokhrel, S.; Bârsan, N.; Weimar, U. Influence of Humidity on CO Sensing with p-type CuO Thick Film Gas Sensors. *Sens. Actuators, B* **2011**, *153*, 347−353.